
Article:
Ibrahim, SF, Pickering, J, Ramachandran, V et al. (1 more author) (2022) Prediction of the Mechanical Deformation Properties of Organic Crystals Based upon their Crystallographic Structures: Case Studies of Pentaerythritol and Pentaerythritol Tetranitrate. Pharmaceutical Research, 39 (12). pp. 3063-3078. ISSN 0724-8741

https://doi.org/10.1007/s11095-022-03314-x

Prediction of the Mechanical Deformation Properties of Organic Crystals Based Upon Their Crystallographic Structures: Case Studies of Pentaerythritol and Pentaerythritol Tetranitrate

S.Fatimah Ibrahim[1,2], Jonathan Pickering[2], Vasuki Ramachandran[2], Kevin J.Roberts[2],*

1 Malaysian Institute of Chemical & Bioengineering Technology (MICET), Universiti Kuala Lumpur, 1988 Vendor City,7800 Taboh Naning Malaysia

2 Centre for the Digital Design of Drug Products, School of Chemical and Process Engineering, University of Leeds, Woodhouse Lane, Leeds, LS2 9JT, United Kingdom

3 School of Computing, University of Leeds, Woodhouse Lane, LS2 9JT, Leeds, United Kingdom

Nomenclature

API: Active Pharmaceutical Ingredients

PET: Pentaerythritol

PETN: Pentaerythritol tetranitrate

NA: Avogadro's number

RMS: Root means square

BFDH: Bravais, Friedel, Donnay, and Harker

List of Symbols

E_{disloc}: Dislocation energy

E_{core}: Dislocation core energy

E_{line}: Dislocation line energy

E_{cr}: Lattice energy

E_{sl}^{hkl}: Slice energy

E_{att}^{hkl}: : Attachment energy

d_{hkl}: Interplanar spacing

A: Dislocation constant

K: Modulus of elasticity

b: Burgers vector

γ: Specific surface energy

Z: Number of asymmetric units

Å: Angstrom

Glossary

Synthons: Atomic pairwise intermolecular interactions

Abstract:

Purpose Development of a quantitative model and associated workflow for predicting the mechanical deformation properties (plastic deformation or cleavage fracture) of organic single crystals from their crystallographic structures using molecular and crystallographic modelling.

Methods Intermolecular synthons, hydrogen bonding, crystal morphology and surface chemistry are modelled using empirical force fields with the data integrated into the analysis of lattice deformation as computed using a statistical approach.

Results The approach developed comprises three main components. Firstly, the identification of the likely direction of deformation based on lattice unit cell geometry; secondly, the identification of likely lattice planes for facilitating deformation through the calculation of the strength and stereochemistry of interplanar intermolecular interactions, surface plane rugosity and surface energy; thirdly, identification of potential crystal planes for cleavage fracture by assessing intermolecular bonding anisotropy. Pentaerythritol is predicted to fracture by brittle cleavage on the {001} lattice planes by strong in-plane hydrogen-bond interactions in the <110>, whereas pentaerythritol tetranitrate is predicted to deform by plastic deformation through the slip system {110}<001>, with both predictions being in excellent agreement with known experimental data.

Conclusion A crystallographic framework and associated workflow for predicting the mechanical deformation of molecular crystals is developed through quantitative assessment of lattice energetics, crystal surface chemistry and crystal defects. The potential for the *de novo* prediction of the mechanical deformation of pharmaceutical materials using this approach is highlighted for its potential importance in the design

of formulated drug products process as needed for manufacture by direct compression.

KEYWORDS Crystallographic Modelling, Synthonic Engineering, Mechanical Properties, Slip Planes, Elastic Anisotropy

1 Introduction

Understanding and predicting the mechanical properties of crystals is important in a wide range of particle formation and process technologies, such as crystallisation filtration, milling, drying and tabletting [1]. Many drug products are formulated through tabletting, so understanding and predicting the mechanical properties of both active pharmaceutical ingredients (APIs) and excipients form an essential component of the pre-formulation development process.

The three most common formulation routes (Figure 1) involved in drug product manufacture involving tabletting are wet granulation, dry granulation and direct compression[2]. Of these, direct compression is the simplest and most cost-efficient route and the one less prone to cross-contamination. Nonetheless, to ensure tablet cohesion, direct compression requires powders with high compressibility and flowability to ensure ingredient homogeneity (Table 1). In addition, the mechanical deformation of crystalline powders is strongly affected by their crystallographic structures, and hence, in direct compression, selecting the appropriate solid form can be critical [3].

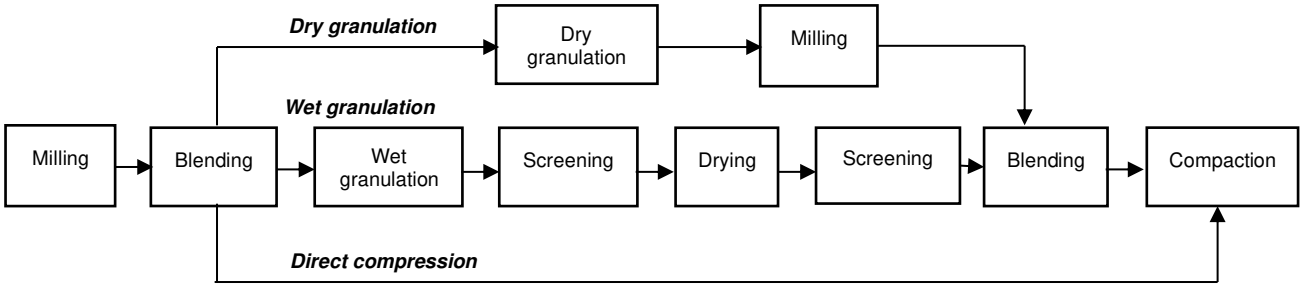

Fig. 1 Schematic diagram showing the three standard route to manufacture pharmaceutical solid dosage forms. The wet granulation is the longest route with the additional unit operations for drying after the wet granulation stage. The direct compression route is the simplest process encompassing just the compression stage after blending [5]

Table 1 Formulation route selection matrix highlighting key particle properties criteria of solid form selection for use in pharmaceutical solid dosage processing, notably the flowability, and compressibility of powders[2]

Flowability	Compressibility	
	High	**Low**
High	Direct compression	Wet granulation
Low	Dry granulation	Wet granulation

Tabletted pharmaceutical dosage form formulations comprise a mixture of API and excipients, with the patient dosage being defined by a combination of their ratio and the tablet weight. Formulation design is governed by ensuring drug product efficacy, safety and processability. If the API content in the formulation is high, the problem of API compressibility issues can become important as many APIs are known to have poor mechanical properties [4] in this respect. In the case of a low dosage of API in the formulation, the mechanical properties of the excipients will tend to dominate, and compressibility issues can be mitigated through a judicious choice of excipients. However, low API loading may lead to API segregation within the formulated blend, resulting in problems in content uniformity. Overall, excipients tend to be rather well-characterised solid forms with well-understood physical and chemical behaviour. Whereas much less tends to be known about the properties of the API, particularly in their early stages of development, highlighting the need for studies that focus on predicting their mechanical properties.

Current experimental methods for assessing the mechanical properties of organic crystals can require significant amounts of experimental characterisation work. The work involves techniques such as atomic force microscopy (AFM)[6], nano-indentation[7], particle rheology and particle flow [8] and single-particle impact studies [4], together with a combination of multiple data analytical approaches, e.g., statistical evaluation[9]. Such studies have also been used in the design and operation of downstream unit operations such as milling [10-12], granulation or compaction[8][13]. Up to now, in-silico prediction of mechanical properties has been much less common. Previous work has emphasised the importance of characterising a material's structure-property relationships. In these, the micro-properties to be considered include intermolecular interactions [3][14-15] , crystallographic structure [16], energetic stability examined using micro/nano-indentation [16-19] and compaction simulation [20-21], inter-molecular energetic analysis and frameworks in particular attachment energy methods [22-23] and topological analysis [24]. In addition, qualitative visualisation methods have been used, notably by assessing the material's crystal chemistry and its slip system availability, both based on the material's crystallographic structure [24-27]. Many API's such as paracetamol [28] and aspirin [4] are known to undergo plastic deformation. The ability of materials to withstand and adapt to stress during the tabletting process relates to the material's propensity to undergo plastic deformation, which would enable the material to flow prior to fracture.

Plastic deformation in ductile organic crystalline materials occurs through the relative movement of layers of molecules, which slide over each other on slip planes (hkl). This translation involves breaking and creating intermolecular synthons within the bulk structure, involving typically van der Waals (vdW) and hydrogen bond (H-bond)

interactions. Planes with larger d-spacings tend to be more close-packed and can, in principle, slip more easily. The interplanar roughness or rugosity will also have an effect as smoother molecular layers are likely to be less constrained to slip.

Molecular shape anisotropy also plays a role in organic materials' mechanical properties, reflecting the fact that translating molecules might entangle and hence interlock during the slipping process. The interlocking of molecules leads to resistance to their motion when strained due to the strong repulsive intermolecular interactions between the molecules involved. In such cases, the more flexible molecules may be able to change conformation, perhaps dissipating any strain energy more effectively. Up to now, there has been no settled predictive modelling strategy and workflow which defines the best approach to characterise the mechanical properties of organic crystals, such as APIs, based on their molecular and/or crystallographic structures [12][24][29-33].

In a previous paper [4], the outline features of the main solid-form attributes contributing to the mechanical deformation of organic crystalline solids were highlighted notably:

- Organic material can be highly anisotropic, with molecules having complex crystal shapes.
- The nature and strength of intermolecular forces can be related to the mechanical deformation of the materials.
- Potential slip planes are likely to have low surface energy and interplanar rugosity, propensity for inter-slip plane interlocking and less breaking of strongest inter-molecular interactions.
- Low crystal symmetry reduces the multiplicity of slip systems and tends to restrict the potential for plastic deformation.

- Likely, deformation behaviour, such as a fracture or plastic deformation, can be understood through detailed characterisation of the deformation slip systems.

This paper builds on this previous work and seeks to develop the foundation of a quantitative model and associated digital workflow by quantifying the above-delineated attributes and integrating these within an assessment of the material's dominant intermolecular (synthonic) interactions. This paper outlines basic deformation theory and the background science underpinning the deformation analysis framework. The overall methodology and computational methods applied are described and demonstrated through complementary case studies on two related compounds, pentaerythritol and pentaerythritol tetranitrate.

2 Basis of the mechanical deformation prediction model

This section provides a brief overview of the underpinning theory relating to the elastic and plastic deformation of organic crystalline solids pertinent to the development of the prediction model.

2.1 Elastic and plastic deformation of organic crystals

Materials can be soft or hard depending on their bulk crystal properties, particularly their symmetry and the strength of their intermolecular interactions. For example, organic compounds, which mostly crystalise in low symmetry systems, tend to have weak intermolecular interactions giving rise to comparatively soft and anisotropic materials.

Materials fracture properties can be characterised as being brittle or ductile. There is no or minimal plastic deformation in a brittle fracture before or during the failure. When this results in a relatively clean fracture surface, this is referred to as cleavage fracture,

and such surfaces are usually characterised by having low surface energy (γ). In ductile fracture, there can be considerable plastic deformation before failure.

A full and detailed description of the plastic deformation process is given in standard texts [34]. Plastic deformation involves the displacement of molecules on their close-packed slip planes {hkl}. This displacement takes place with the assistance of lattice defects such as dislocations which are defined by a 1D translation along the shortest stoichiometric intermolecular distances within the crystal structure. The crystal lattice fault vector associated with dislocation structure is called the Burgers vector ($\overline{b}$). A dislocation slip system for plastic deformation is defined by its combination with a slip plane. The type of dislocation can be characterised by the relative orientation of the Burgers vector with respect to the dislocation line direction ($\overline{\ell}$). For a slip system to be activated during mechanical deformation the crystallographic direction <uvw> of the Burgers vector needs to lie within the slip plane as given by Equation (1) i.e. Weiss zone law analysis [34].

$$hu + kv + lw = 0 \qquad (1)$$

Slip planes are usually the most dense inter-planar plane within the crystal systems, in which slip is enabled by the movement of dislocations. Nonetheless, in organic materials, both the strength and directionality of intermolecular interactions and surface properties of the slip plane can also affect crystal deformation in molecular systems. In particular, the topology of their slip planes may involve having corrugated glide surfaces [35]. This, together with the irregular shape of organic molecules and the anisotropic nature of their intermolecular interactions, makes the deformation process by dislocation slip in organic materials quite complex.

The total energy associated with the formation of a dislocation (E_{disloc}) can be represented by Equation (2) [36].

$E_{disloc} = E_{core} + E_{line}$ (2)

where E_{core} is core energy and E_{line} is the line energy. The former represents short-range non-crystallographic structural disorder around the dislocation line whereas the latter represents the longer-range elastic distortion of the crystal lattice created by the dislocation core. The dislocation core energy can be difficult to estimate directly but usually is estimated to be at least an order of magnitude smaller than the overall line energy [36] and hence, disregarding the core energy component should not cause a significant errors in terms of characterising the overall dislocation energetics.

For isotropic materials, the dislocation line energy can be calculated [36] by Equation (3).

$E_{line} = AK|\bar{b}|^2$ (3)

where K is the modulus of elasticity, |b| is the magnitude of the Burgers vector and A is a constant. This shows that the lowest dislocation energy is consistent with the shortest length of the Burgers vectors. For anisotropic materials, K is not single-valued, and the full elastic tensor notation is required for its accurate description. However, such calculations see e.g. [37-38] are beyond the scope of this current paper.

For a molecular system, the Burgers vector is defined in a similar way as the shortest intermolecular interaction between two molecules related by 3D translational symmetry. Slip within a molecular structure can be expected to start from within a small area and spread outwards [35] and through this generating a slip front with the dislocation line ($\bar{\ell}$) separating the slipped and the unslipped regions. In the lower

symmetry crystallographic systems, which are typical for organic systems, there are fewer opportunities for dislocations to interact (pile-up). Dislocation pile-up may lead to work-hardening, in effect making the material more brittle. Overall, organic systems tend to have a lower number of active slip systems when compared to inorganic materials and their mechanical deformation processes tends to be more complex.

2.2 A mechanical deformation prediction workflow

Building upon the above perspective, a detailed workflow can be developed that encompasses three underlying themes (Figure 2), crystal geometry, crystal chemistry and lattice energetics. Each of these can be predicted and assessed using molecular-scale modelling methods with the output from the various component calculations being integrated and applied to the prediction of the mechanical deformation process using a multiple attributes decision-making (MADM) statistical approach [39]

The model prediction criteria are related to the displacement of planes of molecules along a specified lattice direction. In this, an active slip system occurs when the Burgers vector lies within the slip plane i.e., consistent with ductile behaviour. In cases where the Burgers vector does not lie within the slip plane, then the selected slip system will not be active. Solid forms with potential slip systems which are not active can be essentially classified as being brittle with the potential to undergo either a cleavage or rough fracture. The propensity for cleavage fracture can be assessed through consideration whether the strongest intermolecular interactions within the crystal structure would be broken through the fracture process on the cleavage plane.

Overall, through the integrated analysis presented in Figure 2, solid forms can be characterised in terms of their likelihood for both plastic deformation and cleavage fracture.

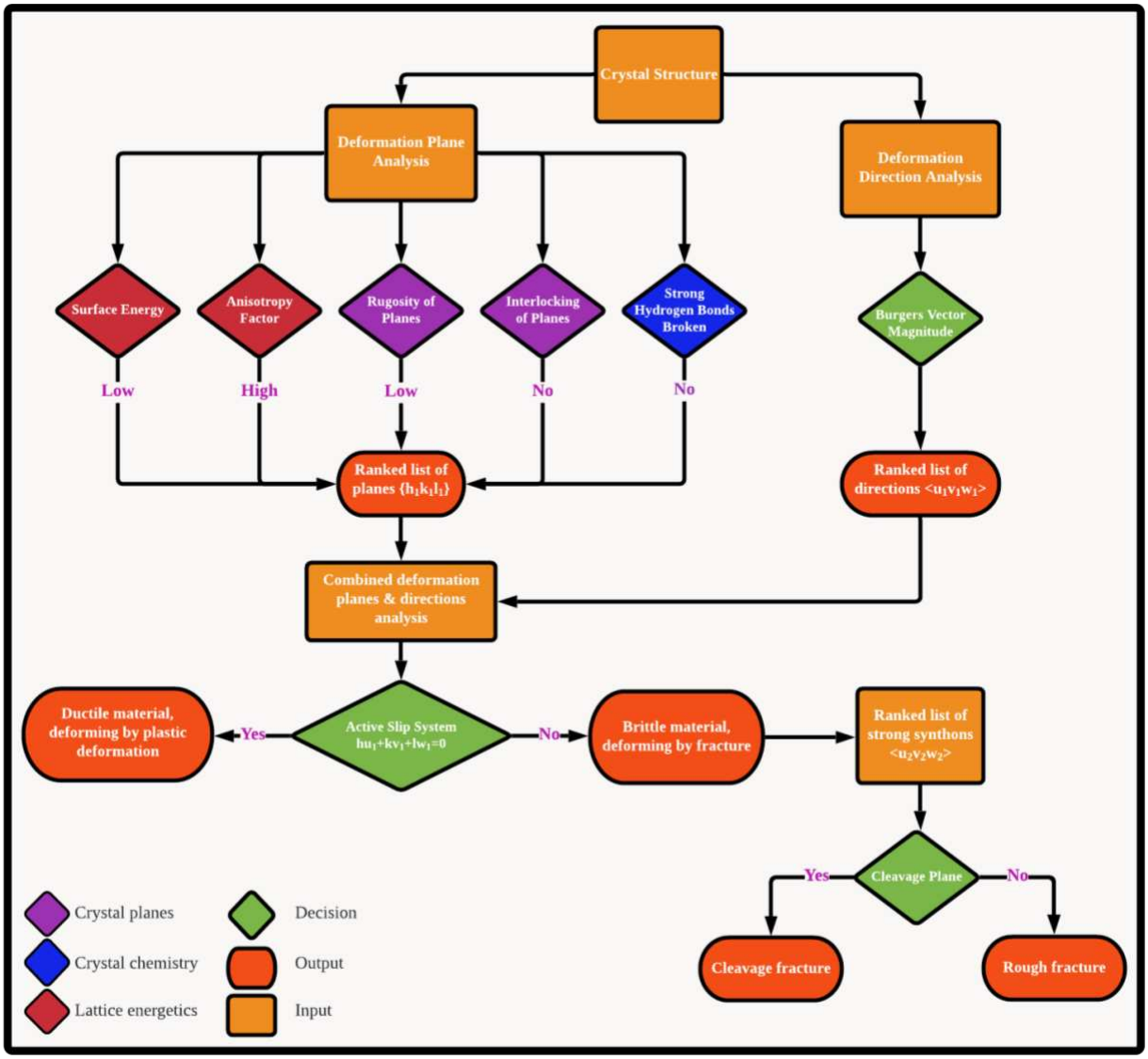

Fig. 2 Diagrammatic workflow for predicting mechanical deformation properties which encompasses three design tools crystal chemistry (blue), lattice energetics (red), crystal planes (purple) where (hkl) is the deformation plane and [uvw] is the deformation direction

2.3 Selection of representative crystallographic structures for mechanical properties case-study

Two closely-related organic crystal systems were considered for methodological evaluation of the proposed workflow in this study; pentaerythritol (PET) and pentaerythritol tetranitrate (PETN). Figure 3 showed the molecular structure for (a) PET and (b) PETN. Although neither compound would be regarded as a pharmaceutical, these two structures are quite representative for the purposes of this study in that they are organic and have intermolecular structures which are dominated by van der Waals, electrostatic and hydrogen bonding interactions.

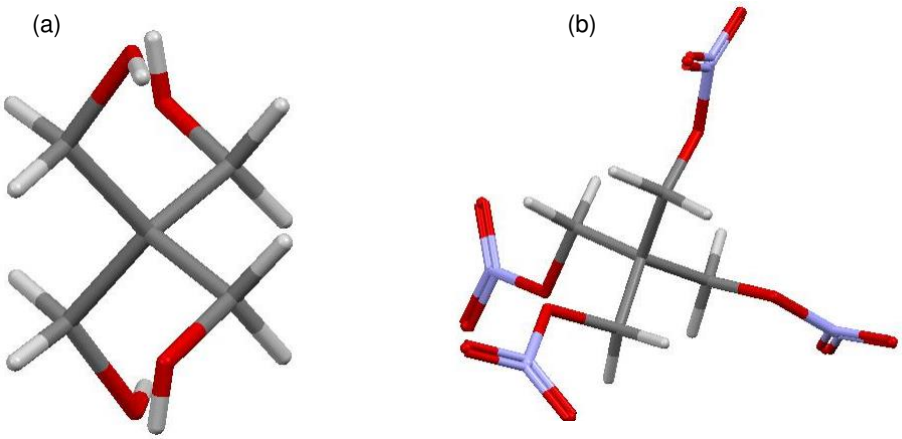

Fig. 3 The molecular structures of (a) pentaerythritol (b) pentaerythritol tetranitrate with oxygen (red), carbon (grey), nitrogen (purple), hydrogen (white).

The PET crystal structure was determined by Eilerman et.al [40] (CSD code PERYO04) and PETN by Zhurova et.al [41] (CSD code PERYTN12). These two crystal structures, as taken from the Cambridge Structural Database (CSD) [42], were of interest because of their contrasting mechanical properties despite the fact that both have similar neopentane skeleton molecular structures and crystallise in tetragonal crystal structures, albeit with a key difference being the Bravais lattice type, whereby PET is body-centred (space group $I\bar{4}$) whilst PETN is primitive (space group $P\bar{4}2_1c$). Both

systems are well-studied with experimental data available for validation of the molecular computational analysis [43-44].

3 Materials and methods

The computational workflow used in this study is summarised in Figure 4.

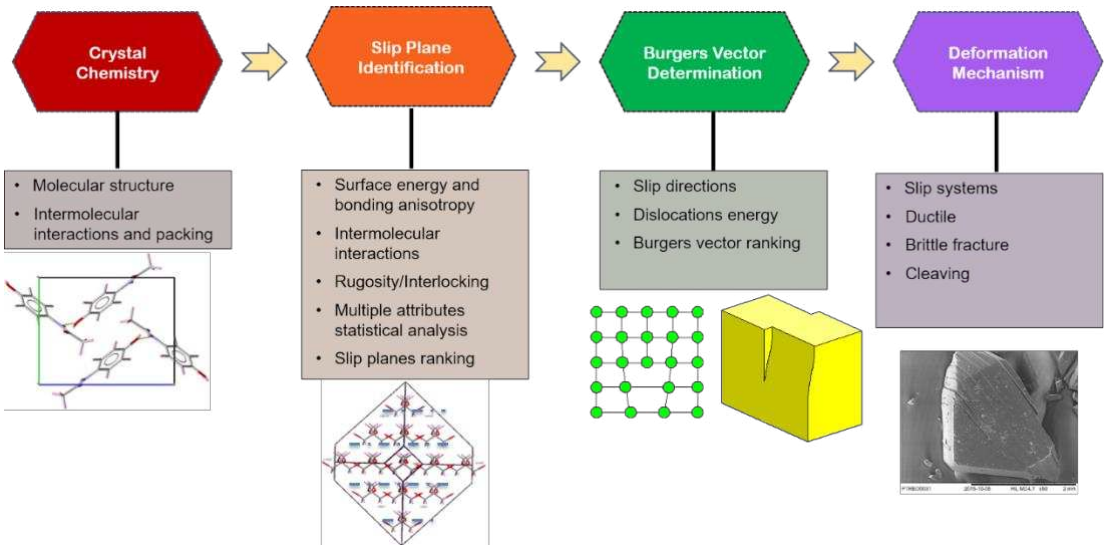

Fig. 4 Computational workflow highlighting the steps involved in predicting crystal deformation mechanism using molecular and crystallographic information

3.1 Crystal chemistry, synthon analysis and morphology

Intermolecular interactions were modelled using the generic empirical Dreiding II force field [45] together with Gasteiger [46] partial charges for the electrostatic interactions. The crystal structure was optimised by minimisation of lattice energy using Forcite module within the Accelerys Materials Studio 5.5 [47] with all the subsequence calculations using minimised molecular structures.

The strength of the individual intermolecular interactions together with their summation for calculating the crystal lattice energies (E_{cr}) were calculated using the atom-atom method as implemented in HABIT98 [48] with an intermolecular summation

radii of between 30 and 60 angstroms (Å). Results from the crystallographic calculations with the limit for zero bond strength is 0.1 kcal.mol^{-1} were used to identify and classify the three strongest intermolecular interactions within the limiting radius.

The calculated lattice energies were compared to experimentally determined sublimation enthalpy, ΔH_{sub}, using Equation (4) [49]

$$E_{cr} = \Delta H_{sub} + 2RT \qquad (4)$$

Where R is the gas constant, and T is the temperature.

The crystal morphology was predicted using attachment energy (E_{att}) approach [50-51] based upon an evaluation of the most likely morphological important habit surfaces using the BFDH method [52]. The surface-terminated intermolecular interactions were assessed by partitioning all the calculated intermolecular interactions contributing to the lattice energy (E_{cr}) between the extrinsic synthons contributing to the attachment (E_{att}^{hkl}) and the fully satisfied surface-stability intrinsic synthons contributing to the slice energies (E_{sl}^{hkl}), see Equation (5) [50].

$$E_{cr} = E_{att}^{hkl} + E_{sl}^{hkl} \qquad (5)$$

The surface anisotropy factor was calculated to assess the degree to which each crystal face is satisfied with respect to its bulk intermolecular interactions by Equation (6) [53-54].

$$\xi_{hkl} = \frac{E_{sl}^{hkl}}{E_{cr}} \qquad (6)$$

The hydrogen bond breaking propensity percentages were calculated on the basis of the hydrogen bond contribution towards attachment energy i.e. that correlated to the hydrogen binding at the surface planes.

3.2 Slip plane identification

Characterisation of slip planes for a given crystal surface (hkl) was carried out by considering a combination of the crystal surface energy, anisotropy factor, rugosity, interlocking of planes and strong synthon breaking. A statistical approach (MADM) was used to weight and rank the potential slip planes.

3.2.1 Surface energy

The specific surface energy (γ) was computed through Equation (7) [50],

$$\gamma = \frac{ZE_{att}^{hkl} d_{hkl}}{2VN_A} \qquad (7)$$

where Z is the number of the asymmetric units in the unit cell; E_{att} is attachment energy; d_{hkl} is the interplanar spacing on the (hkl) face; V is the volume of the unit cell; and N_A is Avogadro's number.

3.2.2 Surface rugosity

The surface rugosity was calculated as a root mean square (RMS) distance based upon deviation of the distance of all atoms within the molecules with respect to an arbitrary plane defined in this case as being at the centre of a slice with a thickness of d_{hkl}. The calculated rugosity values were optimised by allowing the selected plane boundaries to adjust by up to +/- one d-spacing in order to locate the minimum value for the RMS rugosity.

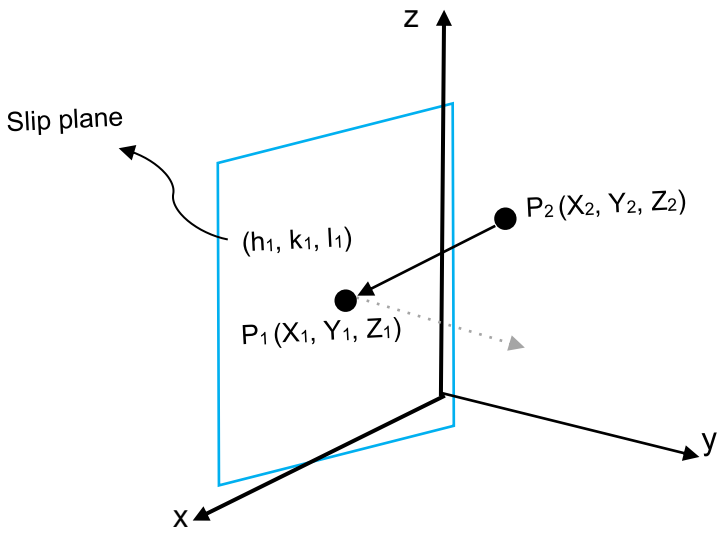

Fig. 5 Schematic showing the basis of the rugosity prediction which encompasses the calculation of the root mean square (RMS) distances of all the constituent atoms within the unit cell from the centre of the designated slip plane

The distance for each atom to a reference slip plane was calculated from the plane to point distance inter-relationship given in Equation (8)[55].

$$d = \frac{|ax_2 + by_2 + Cz_2 + D|}{\sqrt{a^2 + b^2 + c^2}} \qquad (8)$$

As shown in Figure 5, the shortest distance (D) from a point to a plane is along the line perpendicular to the crystal plane i.e., the normal vector direction $\vec{n}(a, b, c,)$. If we denote P1 as the point where the black line segment touches the plane, then P1 (X_1, Y_1, Z_1) is the point on the plane closest to P2(X_2, Y_2, Z_2), the atomic position. The distance is the length of projection of the vector from P1 to P2 onto the normal vector $\vec{n}$. The plane equations can be written as in Equations (9) and (10).

$$ax + by + cz + D = 0 \qquad (9)$$

where

$$D = -ax_2 - by_2 - cz_2 \qquad (10)$$

3.2.3 Slip plane interlocking

The procedure for assessing slip plane interlocking is depicted in Figure 6. Essentially, the dimensional extent of the molecules between two adjacent inter-planar spacings (d_{hkl}) for a specified crystal slip plane (hkl) was measured and expressed as projected distance and the degree of inter-molecular overlap assessed. Through this, a clash factor, defined as the % of inter-planar overlap provided the measure to assess the degree of slip-plane interlock. For example, this might range from substantial intermolecular clash (Figure 6 (a)) to no clash at all (Figure 6(b)).

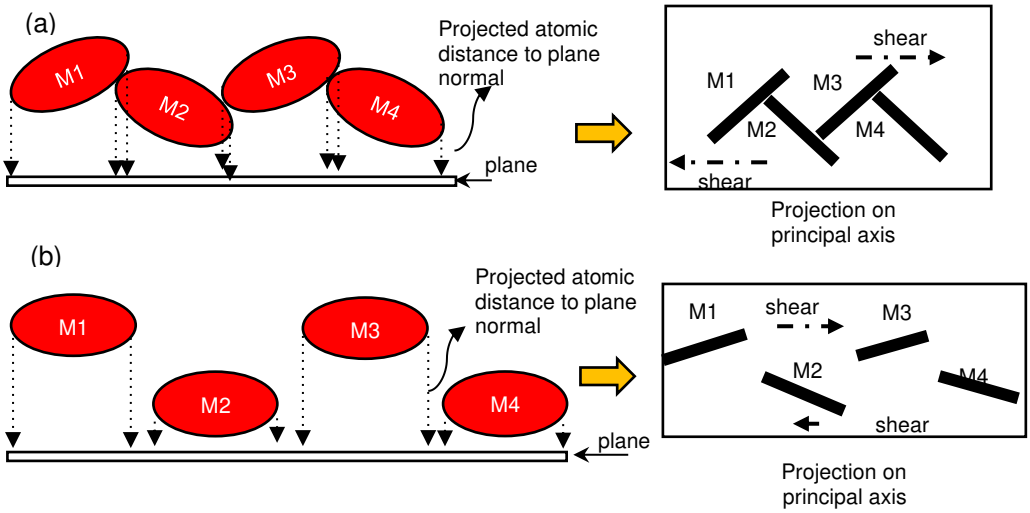

Fig. 6 Schematic diagram showing projection of molecular envelope onto slip plane surface (hkl) highlighting the contrasting cases of inter-plane interlocking where there is (a) and is no (b) interlocking.

3.2.4 Statistical analysis of slip plane criteria

Given the number of criteria considered for the slip-plane analysis, a statistical evaluation was used to provide a fair selection of the most-probable slip planes and the multiple attribute decision-making (MADM) approach was adopted[39]. MADM combined several statistical methods, particularly the weighting method, fuzzy logic and analytic hierarchy process see, for example, Rao and Davim (2008) [39]. In this

study each of the criteria was assigned the same weighting to represent their equal importance. At this early stage of the model's development, the MADM adopted is sufficient to provide a fair judgement to rank the slip planes. The weightings can be adjusted with time as further experimental data becomes available during the research and development process.

3.3 Burgers vector ($\overline{b}$) determination

Likely dislocation Burgers vectors were assessed by measuring the inter-molecular distances for molecules which are related by 3D translational symmetry. For centred Bravais lattices this involved considering the halving of appropriate intermolecular distances within the crystal lattice consistent with the type of crystal lattice centering involved i.e., F, I, A, B or C. After this, the distances were ranked with respect to those having the shortest magnitude, i.e., as would be consistent with the lowest dislocation line energies.

3.4 Deformation mechanistic analysis

In summary, the deformation mechanistic analysis was carried out following the workflow outlined in Figure 2. In this, ductile behaviour was assessed through the criteria described outlined above, notably the identification of a likely deformation plane coupled with the existence of a low energy dislocation lying within the slip plane i.e., meeting Equation (1).

In the absence of a successful meeting of the above criteria, further analysis was carried out to assess the likely nature of crystal fracture in the absence of plastic deformation. In this, the strongest synthons were assessed to see if they were orientated within the deformation plane from which the likelihood of clean cleavage fracture (or otherwise) was assessed.

4 PET case study

4.1 Crystal chemistry analysis

4.1.1 Lattice energy and crystal morphology

The calculated lattice energetics for PET was -32.67 kcal/mol, consistent with the known sublimation enthalpies[56], which are 2 kcal/mol higher, the latter reflecting the difference associated with the temperature at which the sublimation enthalpy was measured. The PET molecule is symmetrical and compact. Therefore, its intermolecular interactions tend to be dominated by interactions between its terminal groups, as can be seen from the contributions from the main functional groups in Table 2.

Examination of the PET structure reveals that the terminal hydroxyl groups of PET contribute most, ca. 72%, towards the lattice energy compared to the neopentane group ca. 28%. A detailed functional interatomic analysis of PET (Figure 7) showed that the major contributor to PET lattice energy is from the hydrogen atoms involved in hydrogen bonding ca. -22.65 kcal.mol^{-1} followed by oxygen ca. -13.49 kcal.mol^{-1} and carbon ca. -5.72 kcal.mol^{-1}. Attachment energy calculations reveal the predicted crystal morphology of PET to be bipyramidal. The morphology was consistent with the experimentally grown crystals, as shown in Figure 8, with the highest habit plane having the surface area face being {101}.

Table 2 The summary of the respective types of intermolecular interactions in PET.

	Functional group	vdW	Coulombic	Total (kcal/mol)	%
PET	**Hydroxyl**	-8.80	-4.20	-13.00	72.00
	Neopentane	-4.28	-0.92	-5.20	28.00

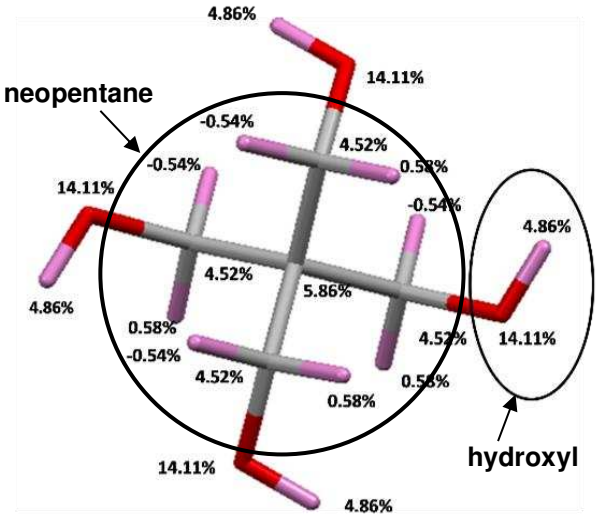

Fig. 7 % atom-atom contributions to the lattice energy of PET for a 10(Å)limiting radius of highlighting the importance of the observed, hydroxyl groups.

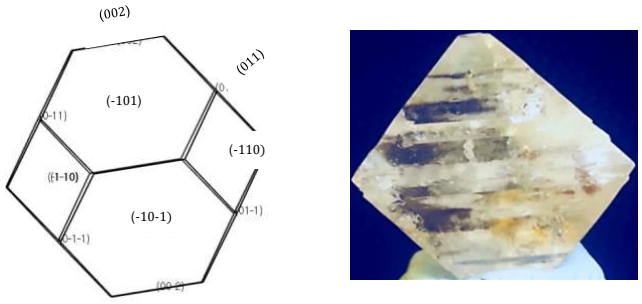

(a) (b)

Fig. 8 The predicted morphology of PET (a) in comparison to the experimentally observed crystals (b).

4.1.2 Intermolecular interactions

The analysis of the intermolecular synthons is summarised in Figure 9 and Table 3. The strongest interactions were provided by (synthons A_1, B_1, and C_1) whose energies were -4.82, -1.21 and -0.32 kcal.mol^{-1}, respectively. The strongest synthon A_1 is aligned along the [010] and [100] directions i.e. being related by the 4-fold axis at an intermolecular centre-to-centre distance of 6.28 Å. The A_1 synthon is associated with OH….HO hydrogen bonding between the hydroxyl groups which act as both hydrogen

bonding donors and acceptors. The intermolecular interaction energy for synthon A_1 is about four times higher than that of synthon (B_1) and might suggest that these strong hydrogen-bonded interactions would dominate the mechanical properties of PET.

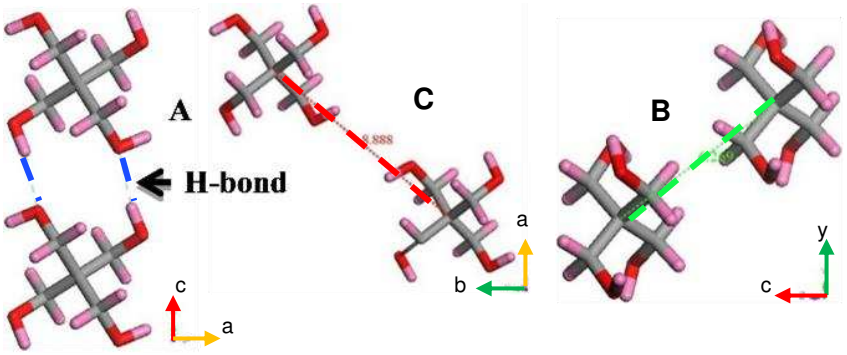

Fig. 9 Identification of the key intermolecular synthons (A, B and C) as extracted from the bulk crystallographic structures of PET highlighting the fact that its strongest interaction (synthon A) involves highly directed hydrogen bonds.

4.2 Analysis of potential slip planes

Qualitative analysis of the crystal packing (Figure 10) for PET revealed a number of potential slip planes, {101}, {011} and {001}, albeit two of these {101} and {011} involved the breaking of hydrogen bonds. Whilst the morphological importance of the habit planes is predicted, the analysis shows that these are not necessarily the material's active slip planes when one considers all the possible combinations of lattice planes for systems such as PET.

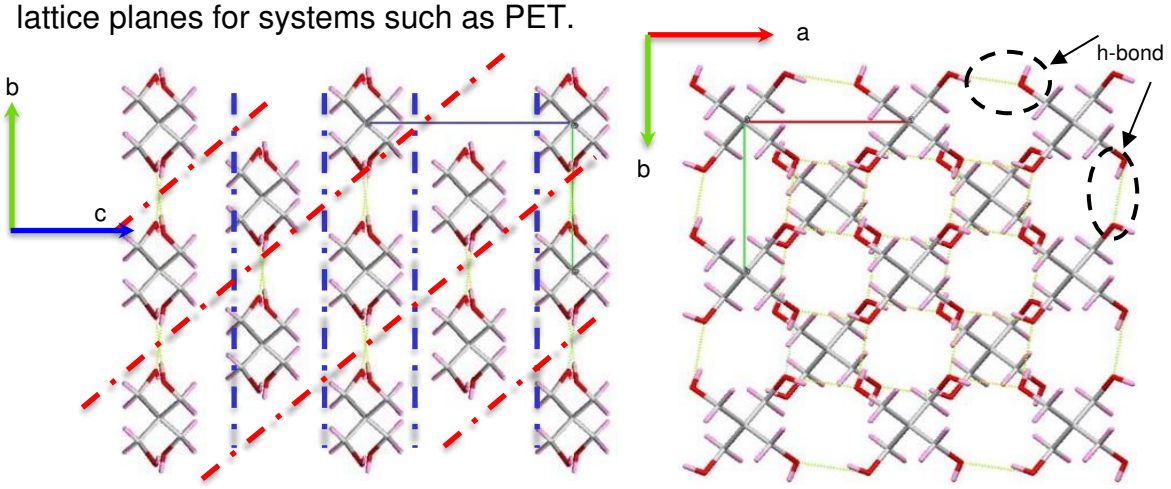

Fig. 10 Intermolecular packing projections for PET viewing the lattice normal to the [100] and [001] directions respectively. The PET structure exhibit a sheet-like pattern when viewed through [100] directions, and H-bonding was identified along the [100] and [010] directions.

Table 3 Characterisation of three strongest intermolecular interactions identified as hydrogen bond (h-bond) and van der Waals (vdW) for PET (A_1, B_1, C_1). The contribution of each interaction towards potential slip plane (hkl) surfaces is also identified.

PET												
Synthon	**Type of interaction**	**Multiplicity**	**Length (Å)**	**Synthon strength (kcal/mol)**	**Synthon direction <$u_2v_2w_2$>**	**{100}**	**{001}**	**{010}**	**{111}**	**{101}**	**{011}**	**{110}**
A_1	**h-bond**	8	6.28	-4.82	<010>	E_{att}	$\boldsymbol{E_{sl}}$	E_{att}	E_{att}	E_{att}	E_{att}	E_{att}
B_1	**vdW**	16	6.27	-1.21	<100>	E_{att}	E_{att}	E_{att}	E_{att}	E_{att}	E_{att}	E_{att}
C_1	**vdW**	8	8.89	-0.32	<110>	E_{att}	$\boldsymbol{E_{sl}}$	E_{att}	E_{att}	E_{att}	E_{att}	E_{att}

Table 4 Analysis of the key slip-plane metrics for PET encompassing surface plane satisfaction, rugosity, surface energy, interlocking of molecular during slip and hydrogen bond breaking.

Name	Face (hkl)	Interplanar spacing (d_{hkl}) m^{-10}	Slice energy (kcal mol^{-1})	% surface satisfaction	Attachment Energy (kcal mol^{-1})	Rugosity (Å)	Surface energy (γ) (kcal/ $Å^2$)	Interlocking	Hydrogen bond breaking	% satisfying MADM	Rank
PET	{001}	8.84	-25.75	81.5	-5.84	3.36	0.15	No	No	94	1
	{101}	5.12	-14.84	47.0	-16.74	3.29	0.13	No	Yes	54	2
	{110}	4.44	-5.56	17.6	-26.04	3.03	0.17	Yes	Yes	33	3
	{111}	3.97	-4.53	14.4	-27.06	3.29	0.20	No	Yes	33	4
	{100}	6.29	-14.78	46.8	-16.82	4.94	0.30	Yes	Yes	25	5

For PET, hydrogen-bonded synthons (A_1) created between the terminal hydroxyl groups were found to contribute toward the slice energy for {001} face (Table 3). This finding correlates well with the high degree of surface satisfaction calculated for {001} surfaces (Table 4).

Analysis of the rugosity data for PET (Table 4) reveals the highest rugosity of 4.94 for the {100} planes, with the lowest being 3.03 for the {110} planes, in good agreement with the qualitative analysis of crystal chemistry given previously. The rugosity for the {001} planes was 3.36. The lowest surface energy for PET was found to be 0.15 kcal.$Å^{-2}$ for the {001} planes, with the highest being 0.30 kcal.$Å^{-2}$ for {100} respectively.

The interplanar interlocking analysis (Table 4) revealed that the molecules on the {001}, {101} and {111} planes do not significantly overlap. In terms of hydrogen bond breaking, only the {001} planes did not have hydrogen bonds protruding from the plane surface. All the other planes exhibited a propensity for hydrogen bond breaking when deformed.

The most unsatisfied face for PET is {111}, with anisotropy values of 14.4%, which is reflected by its higher attachment energy of (Table 4). In contrast, the {001} faces showed the highest surface satisfaction with 81.5% reflecting the fact it would be unlikely to create significant strong bonds with incoming new growth layers. This analysis is in agreement with the rugosity ranking for preferred slip planes as well as the fact that its in-plane deformation would not result in intermolecular interlocking.

Analysis of the ranking for potential slip planes revealed that the smallest deviation from the optimum slip plane attributes was 94% for the {001} planes with the rugosity

and surface energy analysis (Table 4) showing that whilst this surface was not the most atomically smoothest surface, it was the only lattice plane within the PET structure for which slip would not involve the breaking of hydrogen bonds. Such hydrogen bonds tend to be highly directional and relatively strong, and in PET structure they lie parallel to the {001} planes, hence creating strong in-plane interactions optimal for a slip plane when compared to the other planes. Assessing such directionality can play a vital part in predicting the fracture mechanism, mindful that a significant fraction of the lattice energy for this compound results from the strength of its hydrogen bonding intermolecular interactions.

4.3 Analysis of potential slip directions

Given its body-centered structure its shortest Burgers vector was half of the translational vector <111> with this being the preferred direction for lattice displacement by dislocation motion consistent with it having the lowest dislocation energy. In contrast, larger Burgers vectors would involve a greater degree of lattice displacement, with concomitantly higher dislocation energies.

Table 5 List of preferred Burgers vector for PET as ranked using the geometrical magnitude (b^2) criteria with the most preferred Burgers vector being the top value.

	Burgers vector <uvw>	Burgers vector magnitude (b^2) ($Å^2$)	Rank (b^2)
PET	½<111>	39.30	1
	<010>	39.50	2
	<100>	39.50	2
	<001>	78.18	3
	<110>	79.00	4

4.4 Prediction of slip systems

The ranked lists of 5 respective putative slip planes and slip directions were intersected for the PET case, resulting in forty-nine slip systems combinations, with twelve of these being active, i.e., possessing the desired in-plane relationship for the combination of slip plane and direction. The shortest Burgers vector of PET, as shown in Table 5, ½ <111> did not lie in the most likely slip planes {001}, and therefore did not result in an active slip system. Whilst other slip systems would be feasible, they all involved hydrogen bond breaking, which lowered their feasibility. Nonetheless, from the prediction model workflow (Figure 2), such inactive slip systems may further be examined to assess their potential fracture for cleavage depending on the geometric relationship between the fracture plane and the strongest intermolecular bonds.

The strongest hydrogen-bonded synthon (A_1) lies in the <010> direction for PET (Figure 11(a)) and therefore lies within the {001} slip plane, thus enabling cleavage-based fracture to take place. This prediction was in good general agreement with available experimental data, which revealed cleavage plane traces within the bulk crystals and on external fracture surfaces due to chipping, both of which were observed to be parallel to the {001} plane PET (Figure 11(b)). Hence, for PET, cleavage-based fracture was found to be both predicted and observed to occur due to the structure's dominating intermolecular interaction directionality rather than by plastic deformation associated with Burgers vector motion.

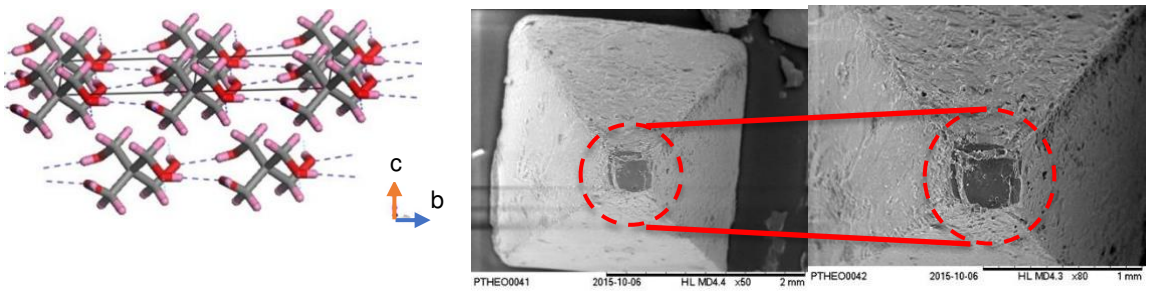

(a) (b)

Fig. 11 Molecular packing diagram highlighting the surface chemistry of the {001} plane in PET highlighting hydrogen bonding in the <010> directions consistent with cleaving of this surface crystal of PET showing chipping of {001} surface consistent with the cleavage fracture.

5 PETN case study

5.1 Crystal chemistry analysis

5.1.1 Lattice energy and crystal morphology

The calculated lattice energy for PETN was found to be -38.61 kcal/mol which was consistent with its experimentally determined sublimation enthalpy. The higher molecular weight associated with the additional nitrate ester functional groups present in the PETN structure is reflected in its higher lattice energy when compared to PET. In a similar manner to PET, the molecular structure of PETN is quite symmetrical. Analysis of the relative contributions from its main functional groups, summarised in Table 6, reveal the terminal nitrate esters functional groups to contribute ca. 97% to its lattice energy and form the structure's dominant functional group (Figure 12). The protrusion of these groups prevent close intermolecular interactions with the molecule's other atoms.

Table 6 Energy contribution summary for each functional group in PETN with 97% energy contributed by nitrate ester group.

	Functional group	vdW	Coulombic	Total (kcal/mol)	%
PETN	**Nitrate ester**	-13.36	-19.07	-32.43	97.00
	Neopentane	-4.36	3.34	-1.02	3.00

The PETN crystal morphology was predicted to be tabular and consistent with the experimentally grown crystals, as shown in Figure 13, with the largest habit planes being {110}.

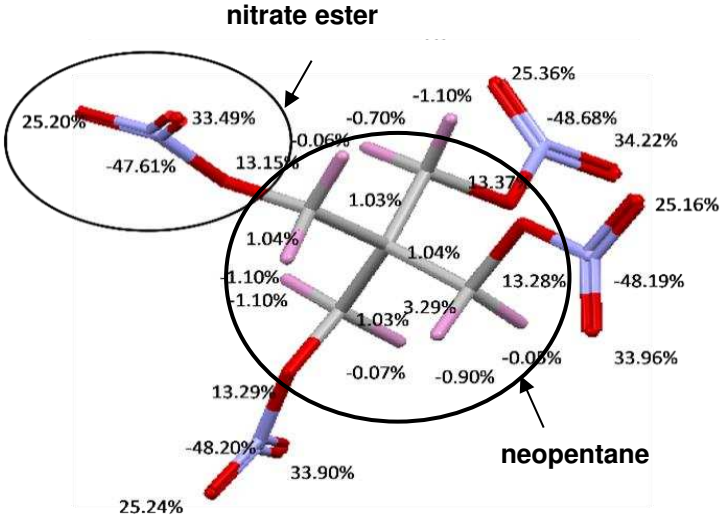

Fig. 12 % Individual atom-atom contributions to the lattice energy of PETN for a 10(Å) limiting radius highlighting the importance of terminal groups.

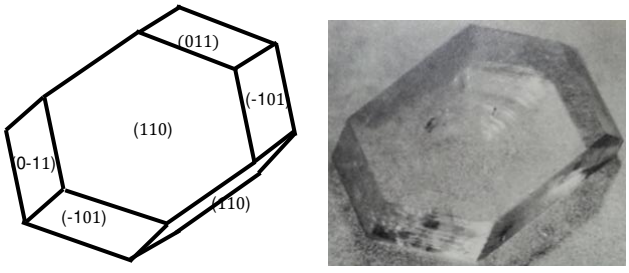

(a) (b)

Fig. 13 The predicted morphology of PETN (a) in comparison to the experimentally observed crystals (b).

5.1.2 Intermolecular interactions

The analysis of the intermolecular synthons in PETN structures is summarised in Figure 14 and Table 7. For PETN, the top three strongest synthons (C_1, C_2, C_3) energies were -3.62, -3.61 and -2.49 kcal.mol^{-1}, revealing the strength of intermolecular interactions to be much more evenly distributed in PETN than in PET, with only small differences of 1% to 4% between their strength. The strongest interactions are comparatively isotropic along the <101>, <100> and <111> directions. More importantly, and in direct contrast to PET, the intermolecular interactions of PETN are dominated by van der Waals interactions while in PET structure they are dominated by stronger and much more directed hydrogen bond interactions.

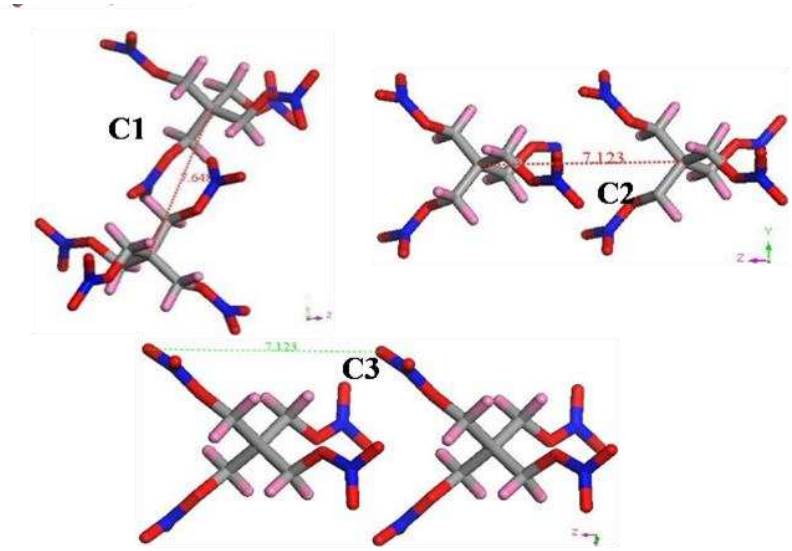

Fig. 14 Identification of the key intermolecular synthons (*C_1, C_2, C_3*) as extracted from the bulk crystallographic structures of PETN highlighting the fact that the strongest interactions involves only isotropic van der Waals interactions.

Table 7 Characterisation of the strongest intermolecular interactions identified as van der Waals (vdW) for PETN. The contribution of each interaction towards potential slip plane (hkl) surfaces is also identified.

PETN												
	Type of interaction	**Multiplicity**	**Length (Å)**	**Synthon strength (kcal/mol)**	**Synthon direction <$u_2v_2w_2$>**	**{100}**	**{001}**	**{010}**	**{111}**	**{011}**	**{101}**	**{110}**
A_2	**vdW**	4	7.65	-3.62	<101>	E_{att}	E_{att}	E_{att}	E_{att}	E_{att}	E_{att}	$\boldsymbol{E_{sl}}$
B_2	**vdW**	4	7.65	-3.61	<111>	E_{att}	E_{att}	E_{att}	E_{att}	E_{att}	E_{att}	E_{att}
C_2	**vdW**	4	7.12	-2.49	<001>	E_{att}	E_{att}	E_{att}	E_{att}	E_{att}	E_{att}	$\boldsymbol{E_{sl}}$

Table 8 Analysis of the key slip-plane metrics for PETN encompassing surface plane satisfaction, rugosity, surface energy, interlocking of molecular during slip and hydrogen bond breaking.

Name	**Face (hkl)**	**Interplanar spacing (d_{hkl}) m^{-10}**	**Slice energy (kcal mol^{-1})**	**% surface satisfaction**	**Attachment Energy (kcal mol^{-1})**	**Rugosity (Å)**	**Surface energy (γ) (kcal/ Å ^{2})**	**Interlocking**	**Hydrogen bond breaking**	**% satisfying MDAM**	**Rank**
PETN	{110}	6.77	-20.41	52.9	-18.14	4.32	0.19	No	No	82	1
	{111}	4.91	-12.38	32.1	-26.17	4.18	0.20	Yes	No	45	2
	{101}	5.71	-15.15	39.3	-24.36	4.01	0.21	Yes	No	43	3
	{001}	7.12	-14.19	36.8	-24.36	5.79	0.27	Yes	No	23	4
	{100}	9.58	-21.58	55.9	-16.98	7.39	0.25	Yes	No	3	5

5.2 Analysis of potential slip planes

A qualitative analysis of the crystal packing (Figure 15) for PETN reveals the only potential slip planes are {110}. All the other likely candidates would involve the potential for intermolecular clashes during any deformation process due to their corrugated surface topologies.

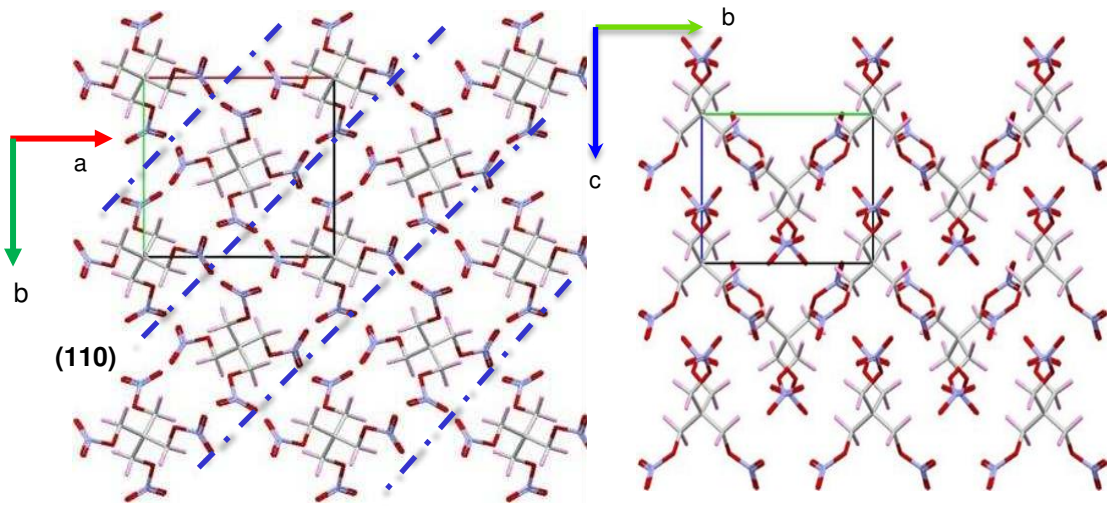

Fig. 15 Intermolecular packing projections for PETN viewing the lattice normal to the [100] and [001] directions respectively. The PETN structure exhibits a zig-zag crystal packing structure when viewed through [100].

For PETN, the vdW synthons (A_2) and (C_2) were found to contribute towards the slice energy for {110} with the (A_2) type having the higher bond strength (Table 7). This correlates well to the high surface satisfaction calculated for the {110} surfaces in PETN. Table 8 shows that the most unsatisfied surfaces were the {111} faces, with an anisotropy value of 32.1% in contrast to the {110} faces, where this percentage was much higher at 52.9%. The most satisfied crystal faces encompasses fewer intermolecular surface binding interactions, consistent with their dominance within the observed crystal morphology.

Analysis of the rugosity data for PETN reveals the highest value (7.39) to be for the {100} faces and the lowest value (4.01) for the {101} faces. The rugosity value for the {110} plane was 4.32.

The lowest surface energy was 0.19 kcal.Å^{-2} for {110} faces and highest was 0.27 kcal.Å^{-2} for {001} face. It can be seen from Table 8 that the {110} faces, whilst having the lowest surface energy, did not have the lowest rugosity value. This is consistent with the calculated values for rugosity and surface energy being quite independent of each other, even though low valuesfor both parameters are preferred for potential slip planes.

The {110} lattice planes were the only planes that were not overlapping, reflecting there being sufficient intermolecular clearance for the slip to occur. This analysis is in good agreement with the preferred {110} planes being found not to interlock.

Overall, the analysis for the PETN slip planes as seen in Table 8, reveals the {110} plane to be the most probable slip plane with 82% fitting attributes for mechanical deformation as the other candidates' scores were below 50%. Compared to PET, the obvious differences in its deformation behaviour can be observed through its more complex crystallographic packing.

5.3 Analysis of potential slip directions

In PETN shortest Burgers vector was in the lattice translational vector of <001> (Table 9), followed by the <010> and <100>. Hence, the <001> vector can be expected to be the preferred vector for PETN slip system analysis. Noting that any plane with indices of the form (hk0) with this Burgers vector would satisfy the Weiss zone law (Equation 1), of which the most preferred potential slip plane will be the {110} planes based on the slip plane analysis.

Table 9 List of preferred Burgers vector for PETN as ranked using the geometrical magnitude criteria (b^2) with the most preferred Burgers vector being the top value.

	Burgers vector <uvw>	Burgers vector magnitude (b^2) ($Å^2$)	Rank (b^2)
PETN	<001>	50.65	1
	<010>	91.74	2
	<100>	91.74	2
	<011>	142.39	3
	<101>	142.39	3

5.4 Prediction of slip systems

The combination of {110} slip plane and <001> slip direction in PETN satisfies the active slip system condition. Based on the workflow proposed in this study, the deformation is predicted to occur by plastic deformation. This outcome agrees with the micro-hardness indentation results of Halfpenny et al. [43], who showed that PET underwent mechanically deformation through this slip system.

The experimental data shown in Figure 16 shows (a) slip traces and well-defined dislocation etch pits after subsequent etching [43]. In the <001> direction no other direction traces were seen from the etching, and slippage was following only one direction. Revisiting the crystallographic structure of PETN (Figure 15), the {110} plane showed good intermolecular clearance without having any significant intermolecular interactions broken perpendicular to the plane. This reflects the strength of the interplanar interactions being weaker than the intraplanar interactions, a situation promoting ease of slippage between the relatively rigid but weakly inter-connected {110} lattice planes.

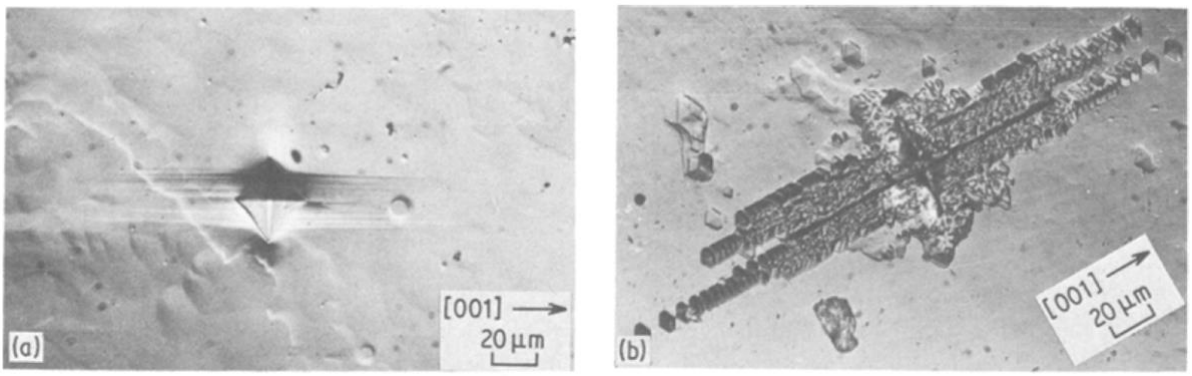

(a) (b)

Fig. 16 Microhardness indentations onto the {110} habit surface of PETN crystals, after reference [43] highlighting well-defined lattice slipping along the <001> direction (a) and showing the same region after acetone etching (b) revealing well-resolved dislocation etch pits. (Figure reproduced with permission from Journal of Materials Science).

6 Conclusions

An integrated molecular modelling-based workflow for analysing the mechanical deformation of organic crystals encompassing deformation by both plastic deformation and/or by cleavage fracture has been developed and tested through case-study work on the related crystal systems of PET and PETN.

Analysis of the mechanical properties of PET revealed deformation by cleavage fracture on the {001} planes enabled by strong in-plane hydrogen-bond interactions in the <110> directions. This demonstrates that the directionality of the strongest intermolecular interactions can also be used to differentiate between crystal fracture by rough interfacial fragmentation and smooth fracture by cleavage particularly in cases where slip systems are not active. In contrast, analysis of the mechanical properties of PETN reveals a strong likelihood for plastic deformation associated with an active slip system of {110} <001> i.e. slip on {110} planes through the motion of dislocations with a Burgers vector of <001>.

This study demonstrates the capability to predict the mechanical deformation of organic crystals materials based on an assessment of combination of a number of the key features shown in the workflow presented in Figure 2 through molecular-based crystallographic modelling. It was found that the correlation between the crystallographic packing arrangements, particularly the way molecules are packed within the crystallographic structure, directs the identification of the primary slip systems within materials and, through this, its overall mechanical deformation process. By such characterisation, ductile or brittle materials, such as the APIs and excipients used within drug products suitable for direct compression, can be determined rationally, aiding and enhancing the overall formulation design process. However, more work is needed to extend the application of these proposed models and workflow for a broader and more diverse range of organic crystalline materials.

Acknowledgements

We gratefully acknowledge the support of the Advanced Manufacturing Supply Chain Initiative through the funding of the 'Advanced Digital Design of Pharmaceutical Therapeutics' (Grant No. 14060) project in terms of supporting the pharmaceutical design modelling research at Leeds. This work also builds upon previous research on morphological modelling supported by the UK's EPSRC (grants EP/IO28293/1 and EP/IO14446/1), as well as the Synthonic Engineering collaborative programme with the CCDC (grant EP/IO28293/1) which was supported also by Pfizer, Boeringer-Ingellheim, Novartis and Syngenta. We gratefully acknowledge Bob Docherty and Klimentina Pencheva at Pfizer and Robert Hammond at Leeds for their interest and support of this work and for many helpful and stimulating discussions. This research forms part of the Ph.D. studies of one of the authors, Siti Fatimah [57], who also wishes to thank the University of Kuala Lumpur for the award of post-graduate study grant.

Conflict of Interest statement

There are no conflicts of interest related to the work reported in this manuscript.

References:

[1] Padma Narayan, Bruno C.Hancock, The relationship between the particle properties, mechanical behavior, and surface roughness of some pharmaceutical excipient compacts, Materials Science and Engineering: A, 2003, 355, 24–36.

[2] Douglas McCormick, Evolutions in direct compression, Pharmaceutical Technology, 2005, 4, 52–62.

[3] Korlakunte V.R. Prasad, David B. Sheen, John N. Sherwood, Fracture property studies of paracetamol single crystals using microindentation techniques, Pharmaceutical Research, 2001, 18, 867–872.

[4] D. Olusanmi, K.J. Roberts, M. Ghadiri, Y. Ding, The breakage behaviour of Aspirin under quasi-static indentation and single particle impact loading: Effect of crystallographic anisotropy, International Journal of Pharmaceutics, 2011, 411(1-2), 49-63.

[5] Loyd V. Allen, Howardd C. Ansel, Ansel's pharmaceutical dosage forms and drug delivery systems, Lippincott Williams & Wilkins, 2013.

[6] Victoria M Masterson, Xiaoping Cao, Evaluating particle hardness of pharmaceutical solids using AFM nanoindentation, International Journal of Pharmaceutics, 2008, 362, 163–171.

[7] Yuanyuan Jing, Yan Zhang, John Blendell, Marisol Koslowski, M.T. Carvajal, Nanoindentation method to study slip planes in molecular crystals in a systematic manner, Crystal Growth & Design, 2011, 11, 5260–5267

[8] J.Prescott, R.J. Hossfeld, Maintaining product uniformity and uninterrupted flow to direct-compression tableting presses, Pharmaceutical Technology. 1994, 18, 98–115

[9] D. Saravanan, Prakash Muthudoss, Praveen Khullar, Rose Venis A, Micronization and Agglomeration: Understanding the Impact of API Particle Properties on Dissolution and Permeability Using Solid State and Biopharmaceutical "Toolbox," Journal of Pharmaceutical Innovation, 2020, 1–16.

[10] P.Narayan, B.C.Hancock, The influence of paticle size on the surface roughness of pharmaceutical excipient compacts. *Materials Science and Engineering: A* **2005**, 226-233.

[11] Gautam R. Desiraju, Designer crystals: intermolecular interactions, network structures and supramolecular synthons, Chemical Communications, 1997, 16, 1475–1482.

[12] C. Malla Reddy, K.Anantha Padmanabhan, Gautam R. Desiraju, Structure-property correlations in bending and brittle organic crystals, Crystal Growth & Design, 2006, 6, 12, 2720–2731

[13] Changquan Sun, David J.W.Grant, Influence of crystal shape on the tableting performance of L-lysine monohydrichhloride dihydrate. *Journal of Pharmaceutical Sciences* **2001**, *90*, 569-579.

[14] Partha Pratim Bag, Miles Chen, Changquan Calvin Sun, C.Malla Reddy, Direct correlation among crystal structure, mechanical behaviour and tabletability in a trimorphic molecular compound, CrystEngComm. 14 (2012) 3865–3867..

[15] Lars Ojamäe, Kersti Hermansson,Roberto Dovesi, Carla Roetti, V.R. Saunders, Mechanical and molecular properties of ice VIII from crystal-orbital ab initio calculations, The Journal of Chemical Physics, 1994, 100, 3, 2128- 2138.

[16] Andrew D. Bond, Pharmaceutical crystallography: is there a devil in the details?, CrystEngComm. 2012, 14, 2363-2366.

[17] Koenraad G.F. Janssens, Dierk Raabe, Ernst Kozeschnik, Mark A.Miodownik, Britta Nestler, *Computational Materials Engineering: An Introduction to Microstructure Evolution*, Academic Press**2010**.

[18] M.S.R.N. Kiran, Sunil Varughese, C.Malla Reddy, U. Ramamurty, Gautam R. Desiraju, Mechanical anisotropy in crystalline saccharin: nanoindentation studies, Crystal Growth & Design, 2010, 10 , 4650–4655

[19] R.I. Ristic, S. Finnie, D.B. Sheen, J.N. Sherwood, Macro-and micromorphology of monoclinic paracetamol grown from pure aqueous solution, The Journal of Physical Chemistry B. 2001, 105, 38, 9057–9066.

[20] J.C. Masteau, G. Thomas, Modelling to Understand Porosity and Specific Surface Area Changes During Tabletting, Powder Technology, 1999, 101, 3, 240–248.

[21] Limin Shi, Changquan Calvin Sun, Overcoming Poor Tabletability of Pharmaceutical Crystals by Surface Modification, Pharmaceutical Research, 2011, 28, 3248- 3255.

[22] Toshiaki Hatanaka, Yasuo Yoshihashi, Katsuhide Terada, Etsuo Yonemochi, Understanding Crystal Cleavability and Physical Properties of Crystal Surfaces using In Silico Simulation. *Chemical and Pharmaceutical Bulletin* **2021**, *69*, 185-198.

[23] Michael J.Turner, Sajesh P. Thomas, Ming W.Shi, Dylan Jayatilaka, Mark A. Spackman, Energy frameworks: Insights into Interaction Anisotropy and the Mechanical Properties of Molecular Crystals. *Chemical Communications* **2015**, *51*, 3735-3738.

[24] Chenguang Wang, Changquan Calvin Sun, Identifying Slip Planes in Organic Polymorphs by Combined Energy Framework Calculations and Topology Analysis. *Crystal Growth & Design* **2018**, *18*, 1909-1916.

[25] Rupeng Bu, Hongzhen Li, Chaoyang Zhang, Polymorphic Transition in Traditional Energetic Materials: Influencing Factors and Effects on Structure, Property, and

Performance, Crystal Growth & Design, 2020, 20, 3561–3576

[26] Torsa Das, Chetan H. Mehta, Usha Y. Nayak, Multiple approaches for achieving drug solubility: an in silico perspective, Drug Discovery Today, 2020, 25,7, 1206-1212

[27] Shenye Hu, Manish Kumar Mishra, Changquan Calvin Sun, Twistable Pharmaceutical Crystal Exhibiting Exceptional Plasticity and Tabletability. *Chemistry of Materials* **2019**, *31*, 3818-3822.

[28] Gary Nichols, Christopher S. Frampton, Physicochemical characterisation of the orthorhombic polymorph of paracetamol crystallised from solution, Journal of Pharmaceutical Sciences, 1998, 87, 6, 684–693

[29] Kohsaku Kawakami, Modification of physicochemical characteristics of active pharmaceutical ingredients and application of supersaturatable dosage forms for improving bioavailability of poorly absorbed drugs, Advanced Drug Delivery Reviews, 2012, 64, 6, 480- 495

[30] Changquan Calvin Sun, David J.W. Grant, Influence of crystal structure on the tableting properties of sulfamerazine polymorphs, Pharmaceutical Research, 2001, 18, 274–280.

[31] Yushi Feng, David J.W. Grant, Influence of crystal structure on the compaction properties of n-alkyl 4-hydroxybenzoate esters (parabens), Pharmaceutical Research, 2006, 23, 1608–1616..

[32] Soumyajit Ghosh, Arobendo Mondal, M.S.R. Kiran, U. Ramamurty, C.Malla Reddy, The Role of Weak Interactions in the Phase Transition and Distinct Mechanical Behavior of Two Structurally Similar Caffeine Co-crystal Polymorphs Studied by Nanoindentation, Crystal Growth & Design, 2013, 13, 4435–4441.

[33] Soumyajit Ghosh, C. Malla Reddy, Elastic and Bendable Caffeine Cocrystals: Implications for the Design of Flexible Organic Materials, Angewandte Chemie, 2012, 51, 41, 10465–10469.

[34] D. Hull, D.J. Bacon, Introduction to dislocations, Pergamon Press Oxford, 1984

[35] Cottrell, *The Mechanical Properties of Matter*, Krieger Publishing**1981**.

[36] Peter M. Anderson, John P. Hirth, Jens Lothe, Theory of dislocations, Cambridge University Press, 2017

[37] H.Klapper, Yu M.Fishman, V.G.Lutsau, Elastic Energy and Line Directions of Grown-in Dislocations in KDP Crystals. *Physica Status Solidi (a)* **1974**, *21*, 115-121.

[38] H.Klapper, *Generation and Propagation of Defects during Crystal Growth*, Govindhan Dhanaraj (editor), Springer Handbook of Crystal Growth, **2010**.

[39] R.V. Rao, J.P. Davim, A decision-making framework model for material selection using a combined multiple attribute decision-making method, The International Journal of Advanced Manufacturing Technology, 2008, 35, 751–760.

[40] D. Eilerman, R. Rudman, Refinement of pentaerythritol, Acta Crystallographica Section B: Structural Crystallography and Crystal Chemistry, 1979, B35, 2458–2460.

[41] Elizabeth A. Zhurova, Adam I. Stash, Vladimir G. Tsirelson, Vladimir V. Zhurov, Ekaterina V. Bartashevich, Vladimir A. Potemkin, A. Alan Pinkerton, Atoms-in-molecules study of intra- and intermolecular bonding in the pentaerythritol tetranitrate crystal., J. Am. Chem. Soc. 2006, 128, 45, 14728–14734.

[42] Frank H Allen, The Cambridge Structural Database: a quarter of a million crystal structures and rising, Acta Crystallographica Section B: Structural Science, 2002, 58, 380–388.

[43] P.J. Halfpenny, K.J. Roberts, J.N. Sherwood, Dislocations in energetic materials 3, Journal of Materials Science, 1984, 19, 1629–1637.

[44] Halfpenny, *A Study of Crystal Defects in Pentaerythritol Tetranitrate and Cyclotrimethylene Trinitramine*, Ph.D. Thesis, University of Strathclyde **1982**.

[45] Stephen L. Mayo, Barry D. Olafson, William A. Goddard, DREIDING: a generic force field for molecular simulations, The Journal of Physical Chemistry, 1990, 94, 26, 8897–8909..

[46] Johann Gasteiger, Mario Marsili, Iterative partial equalisation of orbital electronegativity—a rapid access to atomic charges, Tetrahedron, 1980, 36, 22, 3219–3228.

[47] BIOVIA, Dassault Systèmes[MATERIALS STUDIO], [5.5], SAN DIEGO: DASSAULT Systèmes, [2017].

[48] G. Clydesdale, K.J. Roberts, R. Docherty, HABIT95-a program for predicting the morphology of molecular crystals as a function of the growth environment, Journal of Crystal Growth, 1996, 166, 1-4, 78–83.

[49] J.C. Osborn, P. York, A comparison of sublimation enthalpies with lattice energies calculated using force fields, Journal of Molecular Structure, 1999, 474,1-3, 43–47

[50] P. Hartman, P. Bennema, The attachment energy as a habit controlling factor:: I. Theoretical considerations, Journal of Crystal Growth, 1980, 49,1, 145–156.

[51] Mike Butters, Julie Ebbs, Stuart P.Green, Julie MacRae, Matthew C.Morland, Charles W.Murtiashaw, Alan J.Pettman, Process Development of Voriconazole:A Novel Broad-spectrum Triazole Antifungal Agent. *Organic Process Research & Development* **2001**, *5*, 28-36.

[52] R.Docherty, G. Clydesdale, K.J. Roberts, P.Bennema, Application of Bravais-Friedel-Donnay-Harker, Attachment Energy and Ising Models to Predicting and Understanding the Morphology of Molecular Crystals. *Journal of Physics D: Applied Physics* **2000**, *24*, 89.

[53] H.J. Human, J.P. Van Der Eerden, L.A.M.J. Jetten, J.G.M. Odekerken, On the roughening transition of biphenyl: transition of faceted to non-faceted growth of biphenyl for growth from different organic solvents and the melt, Journal of Crystal Growth, 1981, 51, 3, 589–600

[54] L.A.M.J. Jetten, H.J. Human, P. Bennema, J.P. Van Der Eerden, On the observation of the roughening transition of organic crystals, growing from solution, Journal of Crystal Growth, 1984, 68,2, 503–516

[55] Weisstein E.W., CRC Concise Encyclopedia of Mathematics. 2nd ed.Chapman & Hall/CRC; 2003.

[56] J.S.Chickos, W.E. Acree Jr, Enthalpies of Sublimation of Organic and Organometallic Compounds. *Journal of Physical and Chemical Reference Data* **2002**, *31*, 537.

[57] S. Fatimah Ibrahim, Prediction of the Mechanical Properties of Molecular Crystals Based Upon Their Crystallographic Structure, Ph.D. Thesis University of Leeds, Leeds, 2016.

.